Multiple Scattering Effects on the EXAFS of Ge Nanocrystals

L. L. Araujo[a*], G. J. Foran[b] and M. C. Ridgway[a]

[a]*Department of Electronic Materials Engineering, Research School of Physical Sciences and Engineering, The Australian National University, Canberra ACT0200, Australia. E-mail: lla109@rsphysse.anu.edu.au*

[b]*Australian Nuclear Science and Technology Organisation, Menai, NSW 2234, Australia.*

Synopsis This EXAFS study demonstrates the necessity of a full multiple scattering approach to achieve the most accurate characterization of the structural parameters of embedded Ge NCs.

Abstract We present a detailed Extended X-ray Absorption Fine Structure (EXAFS) spectroscopy study on the influence of multiple scattering effects on the analysis of bulk polycrystalline Ge (c-Ge) and of four Ge nanocrystal (NC) distributions with different mean sizes ranging from 4 nm to 9 nm. We have verified that a complete description of the EXAFS signal up to the third shell of nearest neighbors for both c-Ge and Ge NCs is only achieved by including at least two double scattering (triangular) paths and one triple scattering (collinear) path. Unlike previous reports for bulk semiconductors and Ge-Si quantum dots, our results show that the inclusion of only the most prominent double scattering path is insufficient to accurately ascertain the structural parameters of the second and third shells of nearest neighbors. While for c-Ge the effect is very subtle, for Ge NCs this procedure leads to unphysically small coordination numbers for the second and third shells. The same situation is observed when no multiple scattering paths are taken into account. By analyzing the EXAFS from Ge NC distributions of different mean sizes, the size dependence of the interatomic distance distributions up to the third shell of nearest neighbors has been determined. A greater reduction in coordination numbers and higher structural disorder were observed for the outer shells, reflecting the increase of the surface-to-volume ratio and reinforcing the presence of disorder at the surface induced by reconstruction.

Keywords: EXAFS; multiple scattering; Ge; nanocrystals

1. Introduction

The study of nanoscale systems has attracted much attention due to the unique properties they exhibit (Michalet *et al*., 2005; Linnros, 2005; Roduner, 2006). For example, amorphous silica (a-SiO_2) layers embedded with Ge nanocrystals (NCs), which comprise the system under study in this contribution, emit light (Singha *et al*., 2006) and trap charges (Park *et al*., 2006), making them suitable for the development of new optoelectronic and nonvolatile memory devices. Such properties are critically dependent on the size of the nanostructure where a difference of several nanometres may cause a significant change in the observed properties (Roduner, 2006). Therefore, careful

size dependent studies on the structural properties of nanocrystals are required not only from the fundamental aspect of characterising size and surface related effects but also for the prospect of technological integration.

Extended X-ray Absorption Fine Structure (EXAFS) spectroscopy is a very well suited technique for the study of nanoscale systems, as previously demonstrated (Modrow, 2004; Frenkel, 1999). Since EXAFS probes short range order, it is applicable to both amorphous and crystalline materials, as well as for systems containing different degrees of crystallinity. Structural information for the first nearest neighbour (NN) shell surrounding the absorbing atoms is generally obtained using a single scattering (SS) approach, while information for higher NN shells can only be reliably obtained from a multiple scattering (MS) analysis (Rehr & Albers, 2000). Going beyond the first NN shell in a NC size dependent study is highly desirable for the effects of the higher surface-to-volume ratio are more pronounced for the outer shells. For NCs, where under-coordination of surface atoms and surface reconstruction are expected to increase with decreasing size, the importance of MS effects would in principle be expected to decrease as the particle size decreases. Nevertheless, it has been shown for small Pt NCs (diameters from 2 to 6 nm) that MS effects are not negligible and must be considered (Frenkel, 1999; Frenkel *et al*., 2001). A similar conclusion was suggested for Ge-Si self-assembled quantum dots (QDs) in reference (Sun *et al*., 2005), with the difference that only the most prominent MS path was considered significant. This procedure was based on the analysis of crystalline Ge (c-Ge), where it was argued that including only the most prominent MS path yielded the same results as including that path plus six others.

For this contribution we performed EXAFS measurements for bulk c-Ge and embedded Ge NCs with four different sizes (4, 5, 6 and 9 nm diameters) and analyzed the data with three different approaches to verify the presence and evaluate the importance of MS effects. The case of embedded Ge NCs is particularly interesting because recent X-ray Absorption Near Edge Structure (XANES) analyses suggested that surface reconstruction in this system may happen through the formation of amorphous-like layers (Araujo *et al*., 2007; Araujo, Giulian *et al*., 2007). This would not be completely unexpected, since semiconductors can be amorphised with relative ease and in many cases assume an amorphous structure (unlike metals). Our results indicate that MS effects are present and must be taken into account for all cases. Considering only the most prominent MS path may lead to inaccurate results, especially in the case of Ge NCs. Further characterisation of the NCs with other techniques like Transmission Electron Microscopy (TEM), Small Angle X-ray Scattering (SAXS), Rutherford Backscattering Spectrometry (RBS) and Raman Spectrometry is published elsewhere (Araujo *et al*., 2007; Araujo, Giulian *et al*., 2007).

2. Experimental

Amorphous SiO_2 layers of thickness 2.0 μm were grown on Si (100) substrates by wet thermal oxidation. ^{74}Ge ions were then introduced into the SiO_2 layers by ion implantation at 2.0 MeV to a total fluence of $1x10^{17}$ ions/cm^2 (at liquid N_2 temperature). Afterwards, nanocrystal precipitation and growth were promoted by thermal annealing under forming gas (5% H_2 in N_2). Different combinations of annealing temperatures (between 1060 and 1100 °C) and times (between 20 min and 10 h) were used to yield four different Ge NC distributions with sizes varying from 4.0 to 9.0

nm, as verified by small angle X-ray scattering (SAXS) measurements (Araujo *et al*., 2007). This procedure yields a Ge peak concentration of ~ 3 at.% at a depth of 1.3 μm below the SiO_2 surface, as measured by Rutherford backscattering spectroscopy (RBS) (Araujo, Giulian *et al*., 2007).

After NC growth, samples for fluorescence-mode EXAFS measurements were prepared by removing the Si substrate through a combination of mechanical grinding and selective chemical etching in KOH. The thin SiO_2 layers were then stacked together between kapton tape. This sample preparation method provides both an increased effective Ge areal density and the elimination of scattering from the Si substrate, resulting in a significant improvement in the signal-to-noise ratio and enabling high resolution measurements. A bulk polycrystalline Ge sample suited to fluorescence EXAFS was also prepared, following the method described in (Ridgway *et al*., 2005).

Fluorescence-mode EXAFS measurements at the Ge K-edge (11.103 keV) were performed at beamline 20-B of the Photon Factory, Japan. Experimental spectra were acquired at 15 K and recorded with a 6 x 6 pixel array Ge detector. The Si (111) monochromator was detuned by 50% for harmonic rejection. For energy calibration a c-Ge reference foil was measured in transmission mode at the third ionization chamber concomitantly with the measurement of the fluorescence signal from the samples at the Ge detector.

3. Data analysis

The raw EXAFS spectra were first averaged and energy calibrated to the reference foil signal using the Average 2.0.6 program (Hester, 2007). Next, the EXAFS oscillations were extracted from the experimental spectra by background subtraction (removing the raw absorbance) via the AUTOBK algorithm, as implemented in the ATHENA code (Ravel & Newville, 2005). Figure 1 shows the k^2-weighted EXAFS oscillations for the c-Ge and Ge NCs samples after background removal (where k is the photoelectron wave number). Clearly the signal quality is very good over the measured k-range (16 $Å^{-1}$) even for the smallest Ge NCs. The EXAFS signal for the bulk c-Ge standard was then used to refine the values of the energy shift parameter ΔE_0 according to the procedure suggested in (Kelly & Ravel, 2007). This enabled the alignment of the k-scale of the c-Ge theoretical standard generated by the FEFF8 code (Rehr & Albers, 2000) for all samples and avoided errors in the structural parameters due to a poor choice of the edge energy position E_0. This was performed using the ARTEMIS code (Ravel & Newville, 2005). ATHENA and ARTEMIS are graphical user interfaces (GUIs) for the IFEFFIT code (Newville, 2001). Structural parameters (mean value, variance and asymmetry of the distance distribution) for the first three NN shells were then determined using ARTEMIS. The Fourier transform window used for k space was of the Hanning type, with width 0.8 $Å^{-1}$ and range 4.1 to 15.1 $Å^{-1}$. The window defining the fitting region in the non-phase-corrected radial distance R space was also of the Hanning type, with width 0.2 Å and range 1.5 to 4.8 Å. Effective scattering amplitudes and phase shifts were calculated *ab initio* with the FEFF8 code. Coordination numbers were fixed to bulk values for the c-Ge analysis and fitted for the Ge NCs. Individual interatomic distances were determined for each NN shell instead of relating them all to a single lattice parameter, since experimental evidence shows that due to surface reconstruction the embedded Ge NCs are not well represented by an homogeneous lattice from surface to core (Araujo, Giulian *et al*., 2007).

Individual Debye-Waller factor and third cumulant values were also determined for each NN shell. Each given data set was fitted simultaneously with multiple k weightings of 1–4 to reduce correlations between the fitting parameters. The passive electron reduction factor S_0^2 and the energy shift parameter ΔE_0 were determined from the c-Ge data and kept constant in the Ge NCs fits. The same ΔE_0 was assigned for all paths, since there is no reason to expect charge distribution effects (Haskel *et al*., 1995). The values obtained were $S_0^2 = 0.989 \pm 0.050$ and $\Delta E_0 = 0.291 \pm 1.095$ eV.

Figure 2 shows the Fourier-transformed (k^3-weighted) c-Ge EXAFS experimental spectrum (symbols) up to 6 Å, where the first four NN shells are visible. The vertical dashed lines indicate the region of interest for this work, up to the third NN shell. This choice was based on the fact that further NN shells were not visible in the spectra of the smaller Ge NCs. Together with the experimental spectrum, the first ten photoelectron scattering paths (full lines) as given by the FEFF8 code are also plotted in figure 2. Table 1 lists the atoms involved in each scattering path as well as the half path lengths R_{eff} and degeneracies N. The predicted relevance of each path can be observed in the figure, since it is proportional to their calculated amplitude. The single scattering paths for the first three NN shells (SS1, SS2 and SS3, respectively), superimposed to the experimental spectrum and multiplied by 0.5 in the figure, obviously comprise the dominant part of the EXAFS signal. Nevertheless, the first two double scattering (short triangular) paths, DS1 and DS2, and the first triple scattering (collinear) path TS1 have non-negligible amplitudes. As for the other paths, the second triple scattering path TS2 is still inside the region of interest but has very low amplitude while the further double scattering paths (DS3, DS4 and DS5) have somewhat higher amplitudes but lie mainly outside the fitting region (defined by the dashed lines). Note that all calculated paths shown in the figure have been given a ΔE_0 value of 0.291 eV as determined from the c-Ge sample.

In this study we performed three different fitting procedures to obtain the structural parameters for the first three NN shells. By comparing the results from each approach we will then evaluate the influence of multiple scattering in the EXAFS of c-Ge and Ge NCs. In the first procedure, only the SS paths were taken into account, henceforth referred to as the "No MS" procedure. In the second procedure, called "Full MS", all (seven) paths that lie in the region of interest were used - SS1, SS2, SS3, DS1, DS2, TS1, TS2. In the last procedure, only the most prominent multiple scattering path, DS2, was included together with the three SS paths. This procedure, named "Only DS2", aims to assess the validity of the claim made by Sun and Wei in references (Wei & Sun, 2005; Sun *et al*., 2005) that for bulk binary semiconductors with the zinc-blend structure, as well as for c-Ge and Ge-Si QDs, the inclusion of only the DS2 path yields the same structural parameters as if all multiple scattering paths are included.

For the multiple scattering analyses, not all parameters can be individually floated. We have restrained the MS path parameters as functions of the floating SS path parameters for the shells involved in the respective MS paths. Furthermore, MS paths with the same R_{eff} (DS1 and DS2 - TS1 and TS2) were constrained to have the same Debye-Waller factor and third cumulant values.

4. Results and discussion

4.1. Bulk c-Ge

The structural parameters of the first three NN shells of c-Ge are presented in table 2. Each row shows the results obtained using one of the fitting procedures. The resulting fits are shown in figure 3 together with the experimental spectrum (k^3-weighted) both in Fourier transformed R (top row - a, b c) and in back-Fourier transformed (real part) k (bottom row - d, e, f) space. The slight mismatch between fit and experiment at ~ 4.7 Å and above is assigned to the contributions leaking from paths nominally outside of the R space window (like DS4 and DS5).

As expected, the results obtained for the first NN shell are completely insensitive to the fitting procedure applied, since the first shell is well separated from the region where MS paths play a role. This also indicates that restraining the MS paths as functions of the floating SS paths does not introduce distortions in the results obtained for the SS parameters. There is a small decrease in the fitting errors even for the first shell when MS paths are included in the fits, as apparent from the first three columns of table 2. Furthermore, the statistical "goodness-of-fit" parameters improve significantly when more MS paths are added, as shown in table 3.

Part of this improvement comes simply from the fact that more paths provide more parameters to accommodate the experimental data. None the less, we point out that here all MS parameters are restrained as combinations of the SS parameters, so that adding MS paths does not mean adding free parameters in our case. Furthermore, the concomitant reduction of error bars even for the first NN shell suggests a real improvement in the obtained structural parameters.

The fitting results for the outer shells, on the other hand, have a non-negligible dependence on the fitting procedure, as apparent from table 2 and figure 3 (particularly in the region between the second and third peaks, at ~ 4 Å). This is better visualised from the variation of the Debye-Waller factors σ^2 for the second and third NN shells, plotted in figure 4. If no MS paths are included, the fitting returns virtually the same value of σ^2 for the second and third NN shells. In principle, this is not physically consistent for c-Ge; the third shell σ^2 should be somewhat higher than the second shell σ^2. Including just the DS2 path in the fits is enough to achieve this condition; as mentioned in reference (Sun *et al.*, 2005), DS2 and SS2 interfere destructively and adding DS2 to the fits remedies the higher σ^2 value obtained for the second shell when no MS paths are taken into account. But if the results of the fit including only DS2 are compared with the results of the "Full MS" fit they are not the same, contrary to the suggestion in (Sun *et al.*, 2005). While for the second shell σ^2 they do yield the same value, using only DS2 actually causes a small overestimation of the value of σ^2 for the third shell, as shown in figure 4, for SS3 and DS2 also overlap (figure 2). Therefore, our results for bulk c-Ge indicate that the best fits are obtained only when the "Full MS" approach is used. Finally, we point out that if path TS2 is not included in this approach the results do not change significantly, so that it would suffice to include paths DS1, DS2 and TS1.

4.2. Ge nanocrystals

The structural parameters of the first three NN shells of the four Ge NC distributions are presented in tables 4 and 5. The corresponding fits are shown in figure 5 together with the experimental data in Fourier transformed *R* space (k^3-weighted). All data were plotted in the same vertical scale to clearly show the reduction in amplitude with the decrease in NC size. Despite this decrease in amplitude, both the second and third NN peaks are still visible for the smallest NCs (4 nm diameter). From the figure, it is clear that either the three fitting procedures return very similar structural values for each NC size or the visual aspect of the fits can be deceiving when higher shells and MS paths are involved. A close inspection of the values listed on tables 4, 5 and 6 shows the latter assumption to be correct.

As observed for c-Ge, for all Ge NC distributions the structural parameters for the first NN shell are independent of the fitting procedure, although the error bars are smaller when the Full MS approach is used (see tables 4 and 5). This leads to the same conclusions mentioned for the first shell in the section above.

Regarding the second and third NN shells, a clear difference is apparent between the results returned by each fitting procedure. The effect that was subtle for c-Ge becomes substantial for Ge NCs, as seen from the coordination numbers *CN*, for example. The inadequacy of using only the SS paths is clear due to the much reduced *CN* returned for the second and third shells, as shown in tables 4 and 5 and figure 6.

In figure 6 the structural parameters (symbols) obtained for all samples with the three different approaches are plotted as a function of the NC characteristic sizes. The dashed lines represent the evolution of the coordination numbers according to a geometrical model considering perfectly spherical and crystalline Ge NCs with the diamond structure - they do not account for surface reconstruction. The disagreement between the geometrical model and the experimental data increases dramatically for higher shells, which are most sensitive to surface effects. In fact there is some disagreement even for the first NN shell, but this would be expected in terms of the surface reconstruction in the NCs happening by the formation of an amorphous-like surface layer, as suggested by XANES results (Araujo, Giulian *et al*., 2007) and predicted by molecular dynamics calculations (Pizzagalli & Galli, 2002). Note that for the first shell all atoms in the sample contribute to the EXAFS signal, independent of being at the crystalline core or the reconstructed surface. On the other hand, the surface atoms will not contribute to the signal of the second and third shells if they are in an amorphous-like environment. The non-crystalline fraction of Ge atoms for each sample studied here has been estimated by a linear combination fit using bulk c-Ge and a-Ge as standards, as detailed in reference (Araujo, Giulian *et al*., 2007). Such fractions were then used to correct the geometric model predictions for the second and third NN shells so that surface reconstruction/amorphisation was taken into account in a first approximation. The result of this procedure is shown in figure 6 as the solid lines. It is evident from the figure that the "No MS" fitting procedure yields *CN* values for the second and third NN shells that are too low compared to either the corrected or non-corrected geometric model predictions. If only the most prominent multiple scattering path (DS2) is added to the fit, the *CN* for the second shell improves significantly, but the *CN* for the third shell becomes even smaller at the same time. The best agreement is thus found only when the "Full MS" approach is used, yielding *CN* for the second and third shells which are closer to predicted values.

We point out that, similarly to what is observed for c-Ge, if path TS2 is removed from the "Full MS" fits the results do not change significantly, so that it would suffice to include paths DS1, DS2 and TS1 for Ge NCs as well.

5. Conclusions

By comparing different fitting procedures we have verified that the inclusion of MS paths is essential for a proper evaluation of the structural parameters of the first three NN shells of both c-Ge and Ge NCs. Our results further indicate that the inclusion of two double scattering (triangular) paths - DS1, DS2 - and one triple scattering (collinear) path - TS1 - is the best approach for the systems under study, and that including only the most prominent MS path (DS2) as suggested in reference (Sun *et al*., 2005) is insufficient and may lead to inconsistent results, in particular for the outer shells of Ge NCs. The different conclusion obtained herein relative to previous reports for c-Ge is likely due to the temperature at which the EXAFS measurements were performed. While we measured at 15 K, where thermal vibrations are minimised and a better evaluation of structural parameters is thus possible, in reference (Sun *et al*., 2005) the EXAFS measurements were performed at room temperature, where the amplitude of thermal vibrations is significantly higher and thus so is the variance of the distance distributions.

The fitting results indicate that the first NN shell distances can be determined with a precision better than 0.004 Å for both c-Ge and Ge NCs. This reflects the good quality of the experimental data and the adequacy of using the FEFF8/IFEFFIT theoretical standard and fitting procedures for c-Ge and Ge NCs. For the outer shells this factor is gradually reduced, being ten times worst for the third shell of the 4 nm NCs. In a similar way, increases in the uncertainty of the coordination numbers, Debye-Waller factors and third cumulants are also verified for the outer shells, as expected. Nevertheless, definite trends with size have been identified for the Ge NCs data (figure 6), which illustrate the higher impact on the second and third shells caused by the increase of the surface-to-volume ratio and reinforce the presence of surface disorder induced by surface reconstruction/amorphisation. The physical origin of such trends is described in greater detail elsewhere (Araujo, Giulian *et al*., 2007). For the present report, we have sought to demonstrate the necessity of a full multiple scattering approach to achieve the most accurate characterization of Ge NCs.

Acknowledgements The authors acknowledge the Australian Research Council and the Australian Synchrotron Research Program for financial support. LLA acknowledges the Brazilian Research Agency CNPq for support during his academic formation.

References

Michalet, X., Pinaud, F. F., Bentolila, L. A., Tsay, J. M., Doose, S., Li, J. J., Sundaresan, G., Wu, A. M., Gambhir, S. S. & Weiss, S. (2005). *Science* **307**, 538-544.

Linnros, J. (2005). *Nat. Mater.* **4**, 117-119.

Roduner, E. (2006). *Chem. Soc. Rev.* **35**, 583-592.

Singha, A., Roy, A., Kabiraj, D. & Kanjilal, D. (2006). *Semicond. Sci. Tech.* **21**, 1691-1698.

Park, C. J., Cho, K. H., Yang, W. C., Cho, H. Y., Choi, S. H., Elliman, R. G., Han, J. H. & Kim, C. (2006). *Appl. Phys. Lett.* **88**, 071916.

Modrow, H. (2004). *Appl. Spectrosc. Rev.* **39**, 183-290.

Frenkel, A. I. (1999). *J. Synchrot. Radiat.* **6**, 293-295.

Frenkel, A. I., Hills, C. W. & Nuzzo, R. G. (2001). *J. Phys. Chem. B* **105**, 12689-12703.

Araujo, L. L., Giulian, R., Johannessen, B., Kluth, P., Cookson, D. J., Foran, G. J. & Ridgway, M. C. (2007). *Submitted to Advances in Synchrotron Radiation*.

Araujo, L. L., Giulian, R., Johannessen, B., Kluth, P., Cookson, D. J., Foran, G. J. & Ridgway, M. C. (2007). *Submitted to Physical Review B.*

Ridgway, M. C., Azevedo, G. D., Elliman, R. G., Glover, C. J., Llewellyn, D. J., Miller, R., Wesch, W., Foran, G. J., Hansen, J. & Larsen, A. N. (2005). *Phys. Rev. B* **71**, 094107.

Hester, J. (2007). *Available at http://anbf2.kek.jp/xafs-downloads.html*.

Ravel, B. & Newville, M. (2005). *J. Synchrotron Rad.* **12**, 537-541.

Kelly, S. D. & Ravel, B. (2007). *AIP Conf. Proc.* **882**, 132-134.

Rehr, J. J. & Albers, R. C. (2000). *Rev. Mod. Phys.* **72**, 621-654.

Newville, M. (2001). *J. Synchrotron Rad.* **8**, 322-324.

Haskel, D., Ravel, B., Newville, M. & Stern, E. A. (1995). *Physica B* **208-209**, 151-153.

Wei, S. Q. & Sun, Z. H. (2005). *J. Phys.-Condens. Mat.* **17**, 8017-8028.

Sun, Z. H., Wei, S. Q., Kolobov, A. V., Oyanagi, H. & Brunner, K. (2005). *Phys. Rev. B* **71**, 245334.

Pizzagalli, L. & Galli, G. (2002). *Mat. Sci. Eng. B* **96**, 86-89.

Table 1 Photoelectron scattering paths for the diamond lattice of c-Ge as given by the FEFF8 code. Ge^0 denotes the central absorbing atom and Ge^1, Ge^2 and Ge^3 denote first, second and third NN, respectively. Ge^{1*} denotes a first shell atom in a non-equivalent position to Ge^1.

Notation	Path	R_{eff} (Å)	N (atoms)
SS1	Ge^0 ? Ge^1 ? Ge^0	2.4500	4
SS2	Ge^0 ? Ge^2 ? Ge^0	4.0008	12
SS3	Ge^0 ? Ge^3 ? Ge^0	4.6914	12
DS1	Ge^0 ? Ge^1 ? Ge^{1*} ? Ge^0	4.4504	12
DS2	Ge^0 ? Ge^2 ? Ge^1 ? Ge^0	4.4504	24
TS1	Ge^0 ? Ge^1 ? Ge^0 ? Ge^1 ? Ge^0	4.9000	4
TS2	Ge^0 ? Ge^1 ? Ge^2 ? Ge^1 ? Ge^0	4.9000	12
DS3	Ge^0 ? Ge^2 ? Ge^{1*} ? Ge^0	5.5711	48
DS4	Ge^0 ? Ge^3 ? Ge^1 ? Ge^0	5.5711	48
DS5	Ge^0 ? Ge^3 ? Ge^2 ? Ge^0	5.5711	48

Table 2 Structural parameters - interatomic distances R, Debye-Waller factors σ^2 and third cumulants C_3 - obtained for the first three NN shells of c-Ge by using the three different fitting procedures. The coordination numbers were fixed to bulk values (listed in table 1). The corresponding statistical goodness-of-fit is given in table 3.

Fitting procedure	1^{st} NN			2^{nd} NN			3^{rd} NN shell		
	R (Å)	σ^2 (10^{-3} Å^2)	C_3 (10^{-4} Å^3)	R (Å)	σ^2 (10^{-3} Å^2)	C_3 (10^{-4} Å^3)	R (Å)	σ^2 (10^{-3} Å^2)	C_3 (10^{-4} Å^3)
No MS	2.434 ± 0.005	2.20 ± 0.19	- 0.71 ± 0.60	4.006 ± 0.009	4.61 ± 0.37	1.42 ± 1.27	4.682 ± 0.015	4.67 ± 0.56	-0.33 ± 1.94
Only DS2	2.435 ± 0.003	2.20 ± 0.14	- 0.58 ± 0.44	3.988 ± 0.007	3.93 ± 0.24	-0.36 ± 0.81	4.681 ± 0.012	5.35 ± 0.49	-0.24 ± 1.70
Full MS	2.436 ± 0.001	2.19 ± 0.12	- 0.56 ± 0.30	3.991 ± 0.006	4.01 ± 0.20	-0.10 ± 0.71	4.683 ± 0.009	4.54 ± 0.34	0.13 ± 1.18

Table 3 Statistical goodness-of-fit parameters obtained for the c-Ge fits by using the fitting procedures proposed in this work.

Fitting method	R-factor	Reduced χ^2
No MS	0.0148	85.39
Only DS2	0.0083	45.79
Full MS	0.0059	32.38

Table 4 Structural parameters - coordination numbers *CN*, interatomic distances *R*, Debye-Waller factors σ^2 and third cumulants C_3 - obtained for the first three NN shells of the Ge NCs with characteristic sizes of 9 nm and 6 nm with the fitting procedures specified on each column. The corresponding statistical goodness-of-fit parameters are given in table 6.

		No MS	Only DS2	Full MS
			9 nm NCs	
1st NN	*CN* (atoms)	3.89 ± 0.27	3.90 ± 0.24	3.89 ± 0.14
	R (Å)	2.438 ± 0.004	2.438 ± 0.004	2.438 ± 0.002
	σ^2 (10^{-3} Å^2)	2.91 ± 0.35	2.92 ± 0.31	2.90 ± 0.21
	C_3 (10^{-4} Å^3)	0.44 ± 0.52	0.49 ± 0.46	0.52 ± 0.44
2nd NN	*CN* (atoms)	4.64 ± 1.00	6.81 ± 1.45	7.63 ± 1.48
	R (Å)	3.991 ± 0.013	3.979 ± 0.010	3.984 ± 0.009
	σ^2 (10^{-3} Å^2)	3.08 ± 1.01	4.19 ± 0.94	4.77 ± 0.88
	C_3 (10^{-4} Å^3)	1.99 ± 1.47	0.89 ± 1.27	1.23 ± 1.27
3rd NN	*CN* (atoms)	4.39 ± 2.11	4.14 ± 1.99	6.59 ± 1.29
	R (Å)	4.656 ± 0.029	4.652 ± 0.029	4.677 ± 0.019
	σ^2 (10^{-3} Å^2)	4.83 ± 2.54	5.20 ± 2.61	5.75 ± 1.79
	C_3 (10^{-4} Å^3)	-1.13 ± 3.76	-1.15 ± 3.76	1.63 ± 2.70
			6 nm NCs	
1st NN	*CN* (atoms)	3.66 ± 0.16	3.67 ± 0.12	3.67 ± 0.10
	R (Å)	2.441 ± 0.003	2.442 ± 0.002	2.442 ± 0.002
	σ^2 (10^{-3} Å^2)	3.10 ± 0.22	3.11 ± 0.17	3.11 ± 0.13
	C_3 (10^{-4} Å^3)	0.71 ± 0.32	0.75 ± 0.25	0.76 ± 0.20
2nd NN	*CN* (atoms)	3.93 ± 0.76	6.08 ± 0.99	6.82 ± 0.86
	R (Å)	3.986 ± 0.012	3.974 ± 0.008	3.979 ± 0.007
	σ^2 (10^{-3} Å^2)	4.81 ± 1.01	6.02 ± 0.78	6.65 ± 0.61
	C_3 (10^{-4} Å^3)	1.64 ± 1.51	0.35 ± 1.10	0.66 ± 0.94
3rd NN	*CN* (atoms)	2.63 ± 1.04	2.43 ± 0.82	4.64 ± 0.81
	R (Å)	4.659 ± 0.023	4.655 ± 0.020	4.688 ± 0.011
	σ^2 (10^{-3} Å^2)	4.02 ± 1.90	4.18 ± 1.64	5.30 ± 0.93
	C_3 (10^{-4} Å^3)	0.52 ± 2.78	0.75 ± 2.42	3.67 ± 1.38

Table 5 Structural parameters - coordination numbers *CN*, interatomic distances *R*, Debye-Waller factors σ^2 and third cumulants C_3 - obtained for the first three NN shells of the Ge NCs with characteristic sizes of 5 nm and 4 nm with the fitting procedures specified on each column. The corresponding statistical goodness-of-fit parameters are given in table 6.

		No MS	Only DS2	Full MS
			5 nm NCs	
1st NN	*CN* (atoms)	3.56 ± 0.18	3.58 ± 0.15	3.58 ± 0.14
	R (Å)	2.448 ± 0.003	2.448 ± 0.003	2.448 ± 0.002
	σ^2 (10^{-3} Å^2)	3.52 ± 0.28	3.54 ± 0.24	3.54 ± 0.21
	C_3 (10^{-4} Å^3)	1.05 ± 0.42	1.08 ± 0.35	1.11 ± 0.32
2nd NN	*CN* (atoms)	3.73 ± 0.93	5.99 ± 1.36	6.62 ± 1.28
	R (Å)	3.990 ± 0.015	3.976 ± 0.012	3.980 ± 0.011
	σ^2 (10^{-3} Å^2)	5.66 ± 1.51	7.04 ± 1.22	7.60 ± 1.05
	C_3 (10^{-4} Å^3)	1.38 ± 2.26	-0.22 ± 1.78	-0.12 ± 1.66
3rd NN	*CN* (atoms)	2.39 ± 1.22	2.02 ± 0.97	3.95 ± 1.05
	R (Å)	4.666 ± 0.030	4.659 ± 0.028	4.696 ± 0.016
	σ^2 (10^{-3} Å^2)	4.54 ± 2.73	4.27 ± 2.52	5.32 ± 1.52
	C_3 (10^{-4} Å^3)	0.60 ± 4.03	0.53 ± 3.71	3.77 ± 2.24
			4 nm NCs	
1st NN	*CN* (atoms)	3.24 ± 0.13	3.25 ± 0.11	3.25 ± 0.09
	R (Å)	2.451 ± 0.003	2.451 ± 0.002	2.451 ± 0.002
	σ^2 (10^{-3} Å^2)	3.70 ± 0.22	3.71 ± 0.19	3.71 ± 0.16
	C_3 (10^{-4} Å^3)	1.54 ± 0.32	1.57 ± 0.28	1.59 ± 0.24
2nd NN	*CN* (atoms)	2.72 ± 0.66	4.20 ± 0.96	4.84 ± 0.89
	R (Å)	3.984 ± 0.015	3.975 ± 0.011	3.982 ± 0.010
	σ^2 (10^{-3} Å^2)	5.77 ± 1.42	6.99 ± 1.20	7.88 ± 0.99
	C_3 (10^{-4} Å^3)	2.81 ± 2.12	1.65 ± 1.71	2.24 ± 1.60
3rd NN	*CN* (atoms)	1.24 ± 0.86	1.17 ± 0.79	3.12 ± 0.90
	R (Å)	4.645 ± 0.041	4.633 ± 0.040	4.702 ± 0.018
	σ^2 (10^{-3} Å^2)	4.62 ± 3.61	5.10 ± 3.66	6.71 ± 1.74
	C_3 (10^{-4} Å^3)	-1.28 ± 5.31	-1.89 ± 5.42	4.22 ± 2.61

Table 6 Statistical goodness-of-fit parameters obtained for the Ge NCs fits by using the fitting procedures proposed in this work.

Fitting method	9 nm NCs		6 nm NCs		5 nm NCs		4 nm NCs	
	R-factor	Reduced χ^2	*R*-factor	Reduced χ^2	*R*-factor	Reduced χ^2	*R*-factor	Reduced χ^2
No MS	0.0094	107.29	0.0036	30.86	0.0057	35.54	0.0036	35.58
Only DS2	0.0083	85.51	0.0024	18.36	0.0047	25.12	0.0028	26.31
Full MS	0.0081	77.80	0.0017	11.97	0.0041	20.07	0.0022	19.02

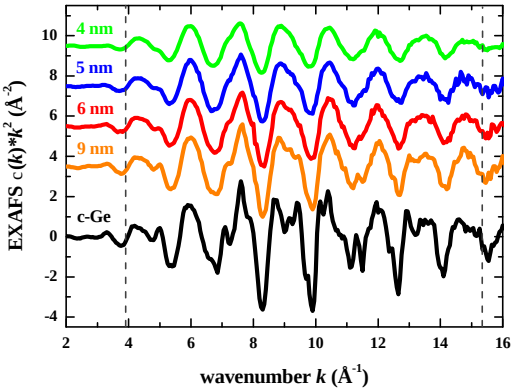

Figure 1 EXAFS oscillations (multiplied by k^2) obtained after background removal for the samples used in this work. Spectra have been vertically shifted for clarity. The dashed lines indicate the *k*-range used for the Fourier transforms.

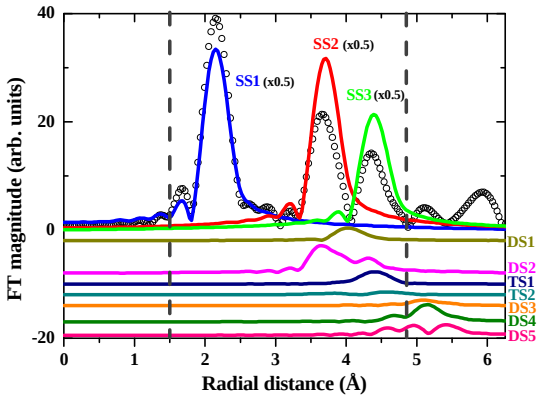

Figure 2 Fourier transformed EXAFS signal measured for c-Ge (symbols) and scattering paths calculated by FEFF8 (solid lines). SS means single scattering, DS means double scattering and TS means triple scattering. The SS paths were multiplied by 0.5 in order to make the figure clearer. The vertical dashed lines indicate the region of interest (up to the third NN shell) in this work.

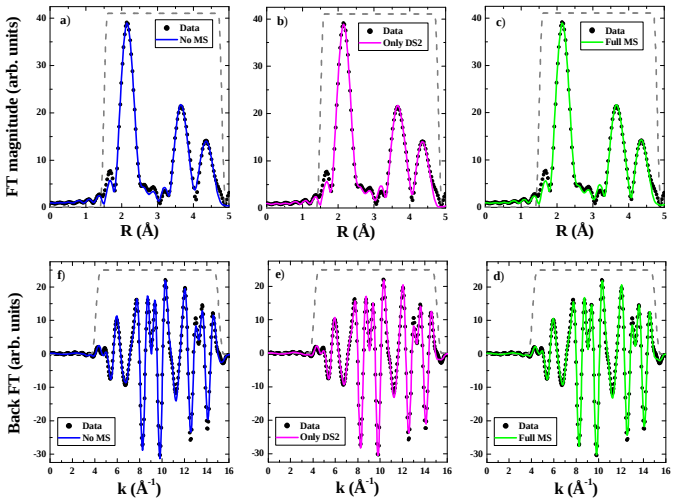

Figure 3 Fourier transformed (top row - a, b, c) and back-Fourier transformed real part (bottom row - d, e, f) EXAFS signal (k^3-weighted) for the c-Ge sample (symbols) and fits using the three procedures proposed in the text, as indicated in the legends. The dashed lines indicate the filtering/fitting windows.

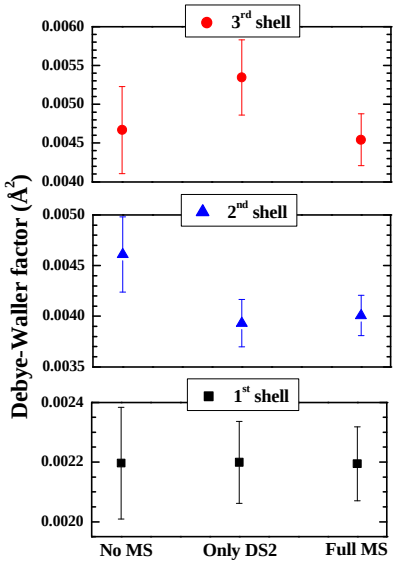

Figure 4 Results obtained for the Debye-Waller factors of the first three NN shells of c-Ge using the fitting procedures specified in the horizontal axis.

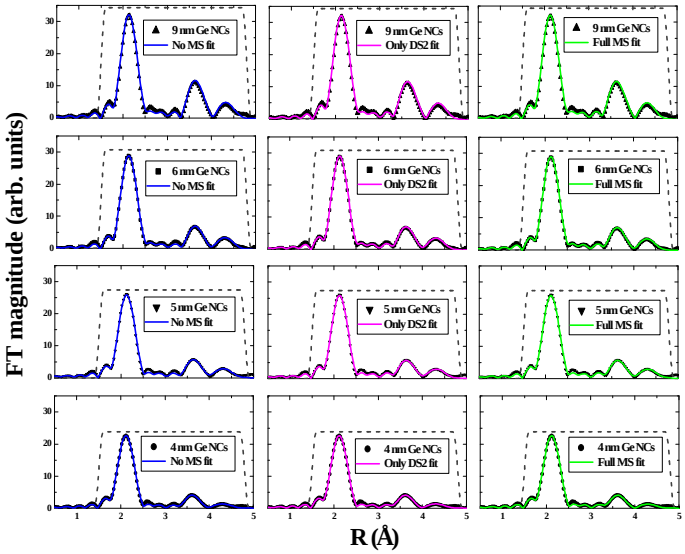

Figure 5 Fourier transformed signal (k^3-weighted) obtained form the EXAFS measurements for the Ge NCs samples (symbols) and respective fits using the three procedures proposed in the text, as indicated in the legends. The dashed lines indicate the fitting windows.

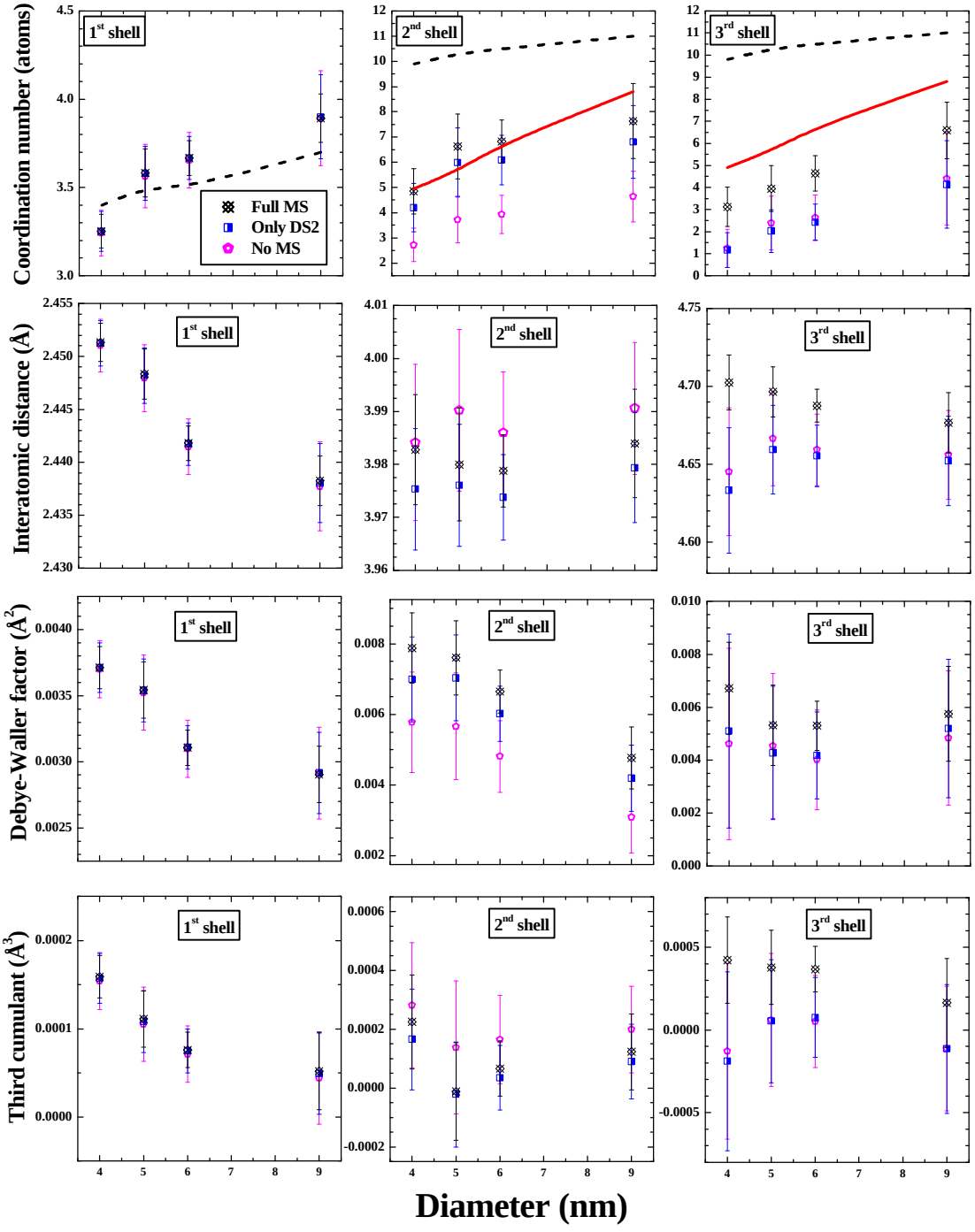

Figure 6 Structural parameters obtained for the first three NN shells of the Ge NCs (symbols) plotted as a function of the NCs characteristic size. Each type of symbol represents one fitting procedure, as specified in the legend. The dashed lines represent the evolution of the coordination numbers according to a geometrical model considering perfectly spherical and crystalline NCs (no surface reconstruction). The solid lines represent the same model corrected according to the fraction of crystalline atoms for each NC size as determined from XANES measurements (Araujo, Giulian *et al.*, 2007).